A Passband-Corrected High Rejection Channel-Select Micromechanical Disk Filter

Mehmet Akgul and Clark T.-C. Nguyen

University at California at Berkeley, Berkeley, California, USA

E-mail: akgul@berkeley.edu

Abstract—The introduction of a 39nm-gap capacitive transducer, voltage-controlled frequency tuning, and a stress relieving coupled array design has enabled a 0.09% bandwidth 223.4-MHz channel-select filter with only 2.7dB of in-band insertion loss and 50dB of out-of-channel interferer rejection. This amount of rejection is more than 23dB better than a previous capacitive-gap transduced filter design that did not benefit from sub-50nm gaps. It also comes in tandem with a 20dB shape factor of 2.7 realized by a hierarchical mechanical circuit design utilizing 206 resonant micromechanical circuit elements, all contained in an area footprint (sans bond pads) of only 600µm×420µm. The key to such low insertion loss for this tiny percent bandwidth is Q's >8,800 supplied by polysilicon disk resonators employing for the first time capacitive transducer gaps small enough to generate coupling strengths on the order of (C_x/C_o) ~0.1%, which is a 6.1× improvement over previous efforts. Defensive strategies built into the array-composite design hierarchy counter process variations via electrical stiffness tuning, and alleviate stress by allocating displacement-buffer devices to increase filter performance and yield. This filter is the first demonstrated that truly offers low insertion loss and high rejection *channel*-selection for ultra-low power communication front-ends targeted for autonomous sensor networks.

Keywords—MEMS resonator, mechanical circuit, quality factor, wireless communications, RF channel-selection, capacitive-gap transducer, frequency tuning, small gap

I. INTRODUCTION

The power consumption of a radio generally goes as the number and strength of the RF signals it must process. In particular, a radio receiver would consume much less power if the signal presented to its electronics contained only the desired signal in a tiny percent bandwidth frequency channel, rather than the typical mix of signals containing not only the wanted signal, but also (often much stronger) unwanted energy outside the channel. The more unwanted energy present, the higher the dynamic range required of the electronics, hence, the larger the power consumption. Unfortunately, a lack of filters capable of selecting single channel bandwidths at RF forces the front-ends of contemporary receivers to accept unwanted signals, and thus, to operate with sub-optimal efficiency.

It is no surprise, then, that attempts to realize RF filters with percent bandwidths on the order of 0.1% sufficient to remove all interfering signals, leaving only energy in the desired RF channel, are abundant in the literature [1][2][3]. Unfortunately, so far none of the explored approaches truly achieves the needed performance, which demands not only small percent bandwidth, but also low passband insertion loss and high stop-band rejection. Several approaches explored
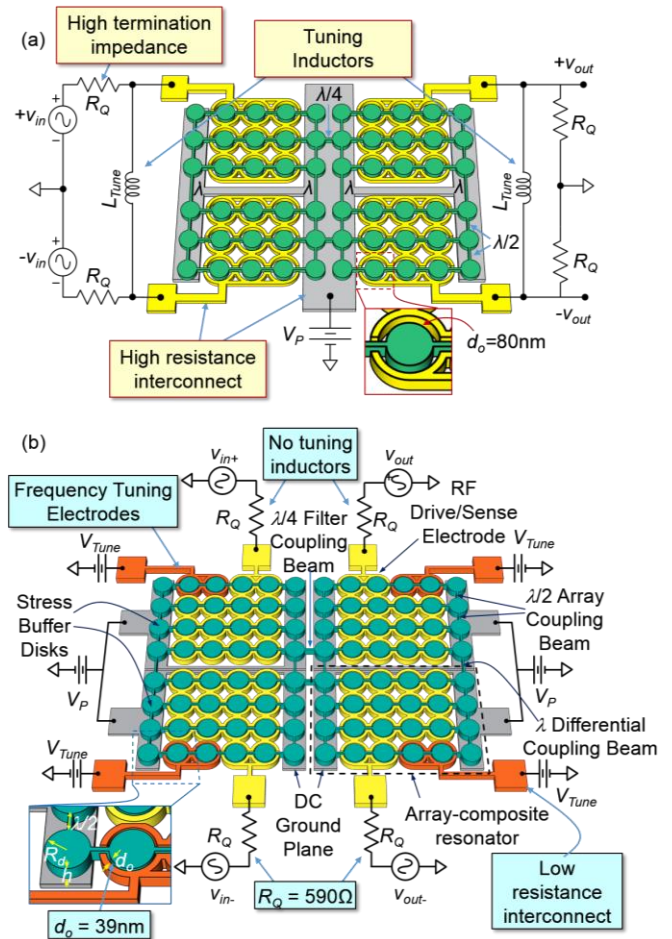

Fig. 1: Comparison of (a) the filter design presented in [1] with labels indicating limitations that hinder performance; and (b) the improved design of this work with indicated improvements; both in preferred bias and excitation configurations used to evaluate filter performance.

thus far use resonators, e.g., based on piezoelectric materials [2][3], that lack the needed Q to achieve low insertion loss in so small a percent bandwidth. On the other hand, approaches that attain sufficient Q's on the order of 10,000, e.g., capacitive-gap transduced resonators, so far do not possess enough electromechanical coupling to attain 50dB stop-band rejection at UHF. In particular, although the design of [1], shown in Fig. 1(a), achieves the needed 0.06% bandwidth with an insertion loss of only 2.5 dB, it does so with only 27dB of stop-band rejection. It also requires rather large termination impedances on the order of 1.5 kΩ that necessitate the use of inductors to resonate out shunt input and output capacitance. Finally, its yield of devices with adequately small passband
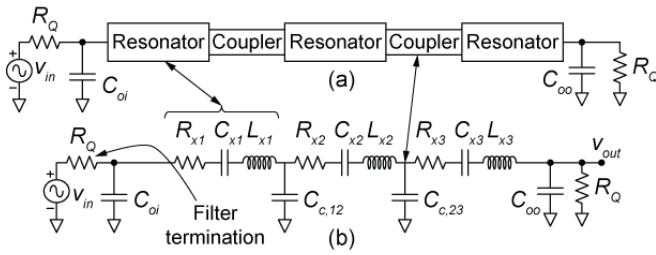
Fig. 2: (a) General topology of a band-pass filter comprising a chain of discrete resonator tanks linked by coupling elements. (b) One implementation for (a) using *LCR* tanks as resonator elements and shunt capacitors as couplers.

ripple is quite low.

Pursuant to fixing these deficiencies, this work modifies the design of [1] to that of Fig. 1(b), which points out the major design changes. Now, smaller electrode-to-resonator gaps on the order of 39nm amplify the input/output electromechanical coupling by more than 8.6×, which directly contributes to larger stop-band rejection and removes the need for inductors. The new design also introduces additional electrodes around disks specifically tasked for frequency tuning towards higher device yield; as well as carefully designed electrode-less buffer devices that alleviate post-fabrication stress, thereby also contributing to higher yield. Combined, these design changes yield a 223.4-MHz two-resonator filter that employs 206 resonant micromechanical elements to realize a channel-selecting 0.09%-bandwidth while achieving only 2.7dB of in-band insertion loss together with 50dB of out-of-channel stop-band rejection. This amount of rejection is more than 23dB better than that of [1] and comes in tandem with a 20dB shape factor of 2.7 commensurate with its use of two array-composite resonators.

II. High Q and Electromechanical Coupling Requirements for RF Channel-Selection

Before expanding on the multi-disk micromechanical filter design, it is instructive to first review some of the basic requirements on the constituent elements of any filter design. Like the majority of narrowband filter realizations, the filter of this work with all its 206 elements essentially takes on a two-resonator version of the topology shown in Fig. 2. Here, a number of identical resonators are linked by coupling elements—in this case shunt capacitors—that serve to spread the frequencies of the identical resonators into a wider pass-band, such as shown in Fig. 3(a). Given that the resonators constitute the main building blocks of this design, it is no surprise that their properties govern what is ultimately achievable by a filter using them.

In particular, any resonator targeting the needs of an RF channel-selecting filter must possess both sufficient Q to prevent undue insertion loss; and enough input/output (I/O) electromechanical coupling to overpower feedthrough currents that would otherwise compromise the filter response. Here, the ratio C_{x1}/C_o [4] from the circuit of Fig. 2 provides a convenient measure of electromechanical coupling strength, the value of which must exceed the fractional bandwidth of the filter to avoid excessive passband distortion. The degree by which it must exceed the fractional bandwidth depends upon the filter type and order, i.e., the number of resonators used.
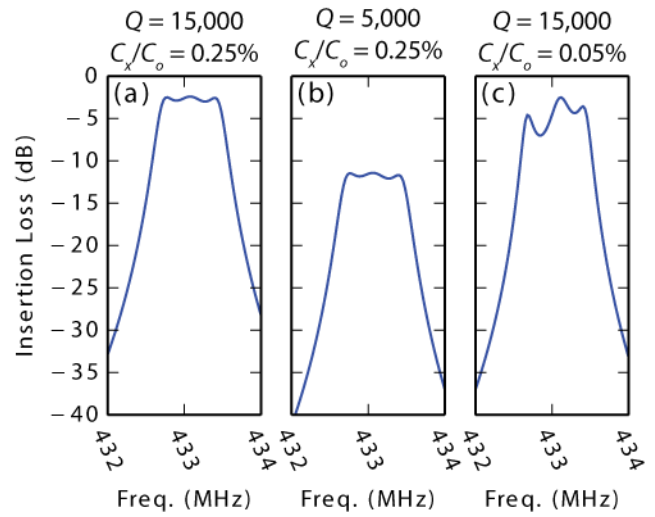

Fig. 3: Simulated frequency responses of a 433MHz three-resonator RF channel-select filter with 0.1% fractional bandwidth for different resonator Q and (C_x/C_o) combinations as (a) $Q = 15,000$ and (C_x/C_o) = 0.25%, (b) $Q = 5,000$ and (C_x/C_o) = 0.25%, and (c) $Q = 15,000$ and (C_x/C_o) = 0.05%.

For example, if the three-resonator filter depicted in Fig. 2 aims to affect a Chebyshev response, then the (C_x/C_o)'s of the I/O resonators must be 2.5× larger than the filter fractional bandwidth.

Fig. 3 illustrates the importance of Q and (C_x/C_o) for an example three-resonator Chebyshev filter, this one centered at 433 MHz with a 0.1% bandwidth. When using resonators with Q's at least 15× the filter Q and (C_x/C_o) at least 2.5× the fractional bandwidth, the desired response in Fig. 3(a) results. A drop in resonator Q from the desired 15,000 to just 5,000 yields the response in Fig. 3(b), which now sports 11.4dB of insertion loss—clearly too much loss. On the other hand, a drop in resonator (C_x/C_o) from the desired 0.25% to 0.05% introduces undue passband ripple, as shown in Fig. 3(c). Clearly, the filter response is good only when its constituent resonators possess sufficient quantities of both Q and I/O coupling.

Note that the needs of a 0.1% RF channel-select filter differ significantly from those of conventional 3% band-select filters used in today's handsets. In particular, while conventional 3% filters put a premium on strong coupling, where (C_x/C_o) ~7% is often needed, and not so much on Q, for which 500 is often acceptable; a 0.1% RF channel-select filter places a high premium on Q, which must often be greater than 10,000, and not so much on (C_x/C_o), for which values on the order of only 0.25% are acceptable.

III. High Q Capacitive-Gap Transduced Disk Array-Composite Resonators

The mechanical filter of this work is much like the filter of Fig. 2, except that instead of *LCR* tanks constrained to Q's below 100, it uses mechanically coupled arrays of vibrating micromechanical resonators [5] capable of achieving Q's exceeding 10,000. As shown in Fig. 4(a), each such resonator comprises an electrically conductive disk surrounded by electrodes spaced by small gap spacing d_o from its perimeter, and supported at its center by a stem post, as described in Fig. 4(c).
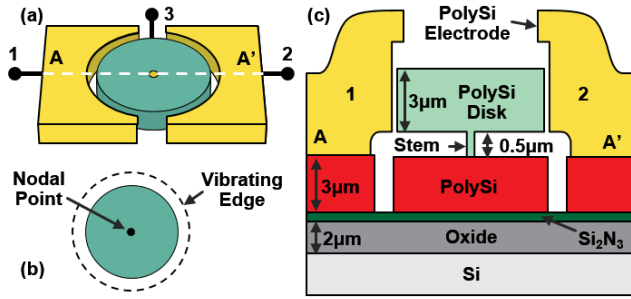
Fig. 4: (a) Schematic description of a contour mode disk resonator, with (b) mode shape and (c) cross-section.

Fig. 5: Schematic description of a λ/2 beam-coupled disk array-composite.

To operate the disk, a dc-bias voltage V_P is applied to its conductive structure (via terminal 3) and ac voltages $v_i = V_i \cos(2\pi f t)$ are applied at each of its electrodes. The combinations of DC and AC voltages applied across each electrode-to-resonator gap generate forces on the disk structure at frequency f that then actuate the disk into vibration with amplitude governed by its high Q force-to-velocity bandpass bi-quad transfer function. In particular, when f matches the disk resonance frequency f_o, the disk responds by vibrating with a large resonance amplitude in the radial-contour mode shape depicted in Fig. 4(b), where the disk expands and contracts around its circumference in a motion reminiscent of breathing. Vibration of the disk gives rise to time-varying capacitors at each electrode-to-resonator interface. Since these capacitors have DC bias voltages across them, they generate currents given by $i_o = V_P \, dC/dt$ that then serve as outputs.

Unfortunately, the tiny size of a single disk relegates it to high impedance. For example, a 6.3μm-radius 433-MHz disk with 100nm electrode-to-resonator gaps and a DC-bias voltage of 15 V posts a motional resistance R_x of 71.8 kΩ which is much too large to match to other system components, e.g., the antenna. To remedy this, the design this work (like that of [1]) employs not one, but several disks with combined inputs and outputs that generate input and output currents larger than that of a single device by a factor equal to the number of disks used. In effect, an array of n disks generates $n\times$ greater output current for the same input voltage amplitude, effectively reducing the overall impedance by $n\times$.

Of course, the currents of the devices in an array sum constructively only if all devices vibrate in phase and at the same frequency. To insure this, as depicted in Fig. 5, the disks in the array are mechanically coupled by half-wavelength beams that effectively transform the array into a single multi-resonator composite device in which all constituent disks vibrate in unison at one mode frequency. Here, the use of half-wavelength coupling links ideally selects one desired mode and rejects all other possible modes. The result: An array-composite resonator with substantially lower impedance and greater power handling than a single one of its constituents.

IV. Overall Filter Structure and Operation

Again, Fig. 1(b) presents a perspective-view schematic of the entire mechanical filter circuit in a preferred differential input/output configuration, showing all applied voltages and term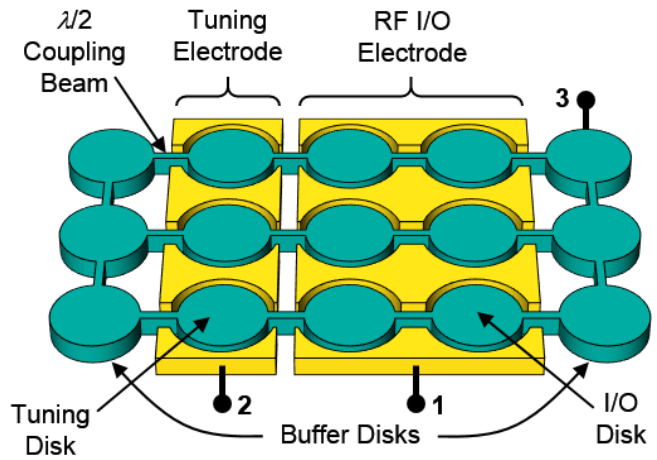ination impedances, and pointing out key differences with the previous one of [1] that allow the present design to achieve much improved performance. As shown, the filter comprises 96 disks mechanically coupled by 110 beams. Many of the disks are surrounded by electrodes spaced only 39nm from their edge sidewalls to serve as either input/output or mechanisms for frequency tuning. Array composite resonators are clearly discernable, and their use represents a first level of hierarchy in an overall hierarchical design reminiscent of those used in complex VLSI transistor circuits, but here used to achieve a complex MSI mechanical filter circuit. There are in fact four levels of hierarchy:

1st Level: Radial-Contour Mode Disk Resonator

The polysilicon contour mode disk resonator depicted in Fig. 4 and described in Section III comprises the unit element and 1st level of hierarchy in the mechanical circuit. In Fig. 1(b), all disks are h=3μm-thick with R_d=12.1μm radii, so share a common radial-contour mode resonance frequency that sets the center frequency of the overall filter.

2nd Level: Disk Array-Composite

To reduce termination impedance and raise stiffness to facilitate small bandwidth, four array-composites of half-wavelength coupled disks make up the 2nd level of hierarchy. Each combines and raises currents, thereby reducing motional resistance, hence, filter termination impedance.

3rd Level: Differential Array-Composite

To enable differential I/O, a 3rd level of hierarchy couples pairs of array-composites via full-wavelength beams. This forces them to vibrate 180° out-of-phase, thereby enabling differential mode operation that cancels feedthrough to enable large stopband rejection.

4th Level: Coupled Resonator Filter

A 4th level of hierarchy couples the differential blocks via quarter-wavelength beams that split their resonances, generating the desired passband and promoting signal subtraction in the stopband that increases rejection.

To operate the filter, a DC voltage is applied to the conductive structure to amplify forces and electrical outputs, and differential electrical inputs are applied through termination impedances (governed by design) to the left-hand terminals.
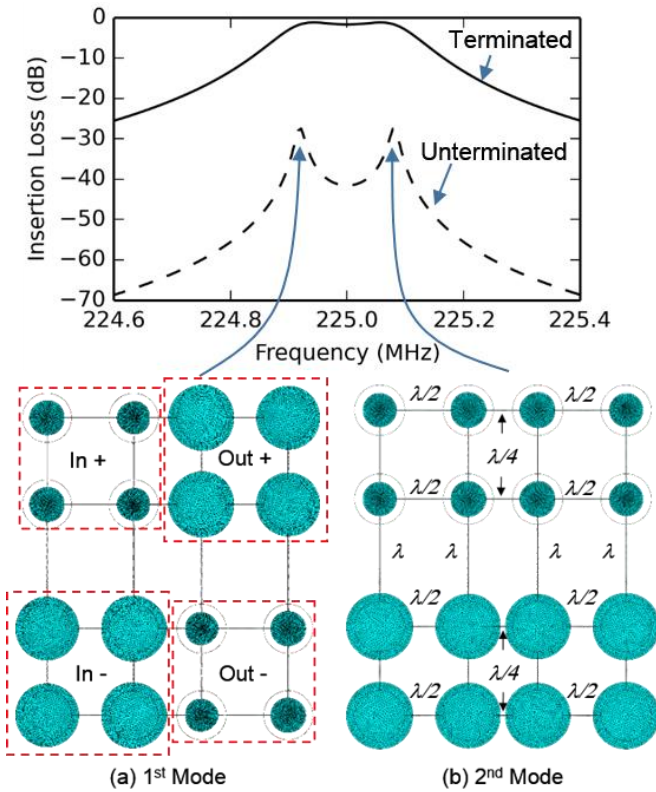
Fig. 6: FEA simulated mode shapes of a two-pole differential coupled disk filter network, where λ/4 coupling beams split the resonances of the coupled differential arrays to (a) out-of-phase and (b) in-phase modes of the system to create the filter passband.

These electrical signals are converted to mechanical (e.g., velocity) signals that are processed mechanically by the frequency response of the structure and then converted back to electrical signals at the outputs.

To visually convey how this rather complicated mechanical circuit functions, Fig. 6 presents the expected properly terminated filter frequency response for a simplified 4-disk-array version this design, with dotted lines to show its unterminated response, and with FEA-simulated vibration mode shapes corresponding to each peak of the response. Here, the mode that actuates the quarter-wave coupling springs the least generates the low frequency peak; while the mode that flexes these couplers the most specifies the high frequency one. When the filter is terminated, loading of the resonators widens their frequency response spectra, allowing them to add constructively between peaks and subtract outside, yielding the desired filter response.

V. FIXES TO PREVIOUS DISK ARRAY FILTER DEFICIENCIES

As can be seen from Fig. 1, many aspects of the design and operation of the current filter are identical to those of [1]. This is for good reason: [1] is an excellent design. Thus, for more details on design and operation, we refer the reader to [1]. This leaves more room to focus the present discussion on the key differences between the two designs that allows the new one to perform so much better.

The utility of the changes made to improve filter performance are perhaps best conveyed by first better describing the

deficiencies with the previous disk array filter design of [1]. As already mentioned, the design of [1] has no issue with insertion loss, since it utilizes capacitive-gap transduced disk resonators capable of Q's >10,000 at its center frequency. Rather, its problems derive more from insufficient transducer coupling and yield loss.

A. Insufficient Electomechanical Coupling

With 80 nm electrode-to-disk resonator gaps seen in the zoom-in of Fig. 1, the coupling factor (C_x/C_o) for the base device used in [1] was only 0.02%. This of course is too small to support even its tiny filter bandwidth of 0.06%, so shunt inductors were employed across its I/O terminals to eliminate C_o as much as possible, thereby greatly increasing (C_x/C_o). It should be noted that use of an inductor here is not an unreasonable approach. Indeed, many of the proposed application scenarios utilize banks of filters hooked in parallel to cover a range of frequencies. In this strategy, the input capacitors of all devices add to generate one much larger capacitor that does not change as filters are switched on or off, so can be resonated out via a single inductor [6].

Still, if only a few filters were needed instead of a large bank, it would be good to avoid the addition of an inductor (or two) to the bill of materials for a cost-driven wireless circuit. In this case, the filter must attain sufficient (C_x/C_o) on its own, without an inductor, and this is best accomplished by increasing I/O transducer strength. To this end, one can quickly observe that the arraying of resonators used in this design does not improve the (C_x/C_o) ratio, since it raises both C_x and C_o simultaneously. Rather, the main utility of arraying is to reduce impedance and raise power handling and linearity—three very important characteristics in their own right, but not solely tied to transducer coupling.

The available knobs to improve (C_x/C_o) are perhaps best revealed via its expression:

$$\frac{C_x}{C_o} = \frac{V_P^2}{d_o^3} \frac{\varepsilon_o R_d \theta_{ov}}{\pi^3 K^2 \chi E} \qquad (1)$$

where ε_o is the permittivity of free space; R_d is the disk radius; θ_{ov} represents the electrode-to-disk overlap angle in radians; E is the Young's modulus of the disk material; χ relates the static mass of the disk to its dynamic mass and equals $\chi=0.763$ for the fundamental contour vibration mode [7]; and K is a dimensionless frequency parameter that depends on the Poisson ratio of the structural material. For polysilicon, $K = 0.654$ [7]. Here, the dc-bias voltage V_P and spacing d_o across the I/O electrode-to-resonator gaps are clearly the strongest knobs, the former having a quadratic effect, the latter a whopping third power influence. Given these dependencies, shrinking the gaps from the 80 nm of [1] to the present 39 nm delivers an 8.6× improvement in (C_x/C_o); and accounting for the radius term in (1) leads to a total improvement by 6.1×. The (C_x/C_o) goes from the 0.02% of [1] to 0.12%, which for the present two-resonator 0.1% bandwidth filter, is plenty sufficient.

One consequence of smaller gaps is a higher susceptibility to stress, where now even small stresses can push a disk into its electrodes, shorting them out and debilitating the whole filter. Here, the stress-relieving electrode-less buffer devices
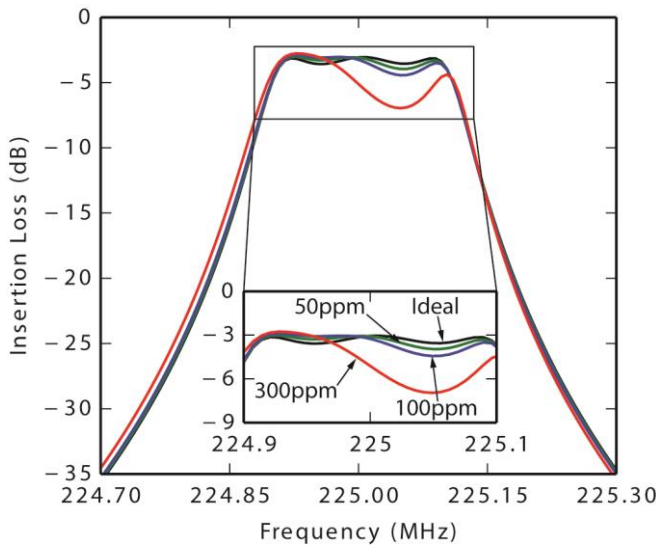
Fig. 7: Simulated frequency response spectra for a 225-MHz three-pole, i.e. three-resonator, 0.5dB-ripple, Chebyshev filter with 0.1% bandwidth, for different amounts of resonator-to-resonator mismatching. For each mismatch case, adjacent resonators experience the indicated frequency deviation in opposite directions to simulate the worst case mismatch scenario.

at the edges of the arrays become even more important to prevent stress-based yield loss.

B. Low Yield

Small percent bandwidth filters present challenges in not only insertion loss, but also yield and repeatability. Indeed, the smaller the percent bandwidth, the smaller the allowable mismatch between resonators. For example, as illustrated by the simulations of Fig. 7, 0.1% bandwidth requires resonator-to-resonator frequency matching to better than 50 ppm to constrain mismatch-added passband ripple to less than 0.5dB over the designed 0.5dB. So far, single disk resonators (such as used in this work) post frequency standard deviations on the order of 316 ppm [8], which is clearly short of the requirement. For this reason, only a small number of the mechanical filters fabricated in [1] actually had acceptable pass-band distortion. Yields of course must be much higher if high volume production is needed.

From [8], it is true that array-composites of resonators can be manufactured with better matching than any one of their constituents, by a factor equal to $\sqrt{n}$, where n is the number of resonators in the array. Thus, the 24 resonators (including non-I/O ones) used in each differential array-composite pair of Fig. 1(b) should improve the standard deviation by 4.9× to 64.5 ppm. Unfortunately, this is still not sufficient.

To combat device mismatch, the present design purposely uses two of its 24 array resonators not for I/O, but rather for frequency tuning by the well-known voltage-controllable electrical stiffness across their electrode-to-resonator gaps [9]. Since only two out of 24 devices are employed this way, the amount of frequency pull is not large, on the order of 3 ppm/V. This, however, is sufficient to traverse the expected (64.5-50=14.5) ppm frequency pull needed to correct for differential array-composite pair mismatch, and thus, is sufficient to correct mismatch-generated passband distortion towards higher manufacturing yields.
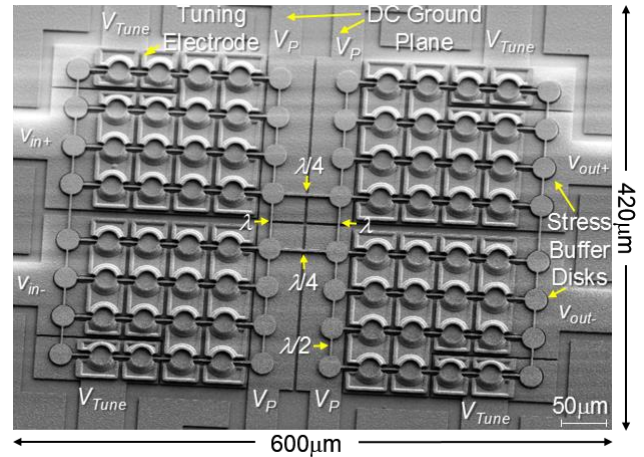

Fig. 8: SEM image of the fabricated and measured differential filter.
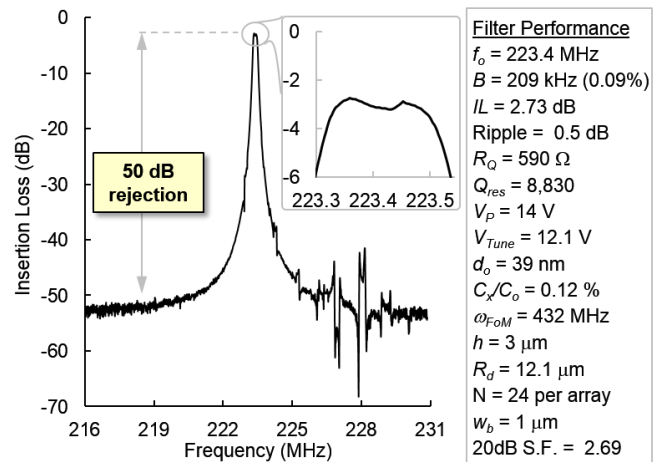

Filter Performance
f_o = 223.4 MHz
B = 209 kHz (0.09%)
IL = 2.73 dB
Ripple = 0.5 dB
R_Q = 590 Ω
Q_{res} = 8,830
V_P = 14 V
V_{Tune} = 12.1 V
d_o = 39 nm
C_x/C_o = 0.12 %
ω_{FoM} = 432 MHz
h = 3 µm
R_d = 12.1 µm
N = 24 per array
w_b = 1 µm
20dB S.F. = 2.69

Fig. 9: Measured terminated filter spectrum with inset zoom-in on the passband. Design parameters are given in the right-hand table.

VI. EXPERIMENTAL RESULTS

Pursuant to verifying the overall design strategy, micromechanical filters were fabricated using a small-gap polysilicon surface micromachining process similar to that of [1] but this time using very thick interconnect lines (*cf.* Fig. 4(c)) to reduce parasitic resistance. Fig. 8 presents the SEM of a fabricated filter matching the design of Fig. 1(b).

The fabricated differential filter was measured using the scheme of Fig. 1(b) realized via the four-port measurement mode of an Agilent E5071C network analyzer with measurement plane moved to the bond-pads using standard SOLT calibration. A dc-bias of V_P = 14V applied to the conductive structure results in needed termination impedances of only 590Ω. DC voltages are also applied to the indicated frequency tuning pads that direct them to electrodes capable of tuning frequency via voltage-controllable electrical stiffness.

Fig. 9 presents the tuned and terminated filter spectrum with an inset zoom-in on the passband showing a 209-kHz bandwidth at 223.4 MHz, i.e., 0.09% bandwidth, with only 2.7dB insertion loss, 0.5dB ripple, and a 20-dB shape factor of 2.7. Small gaps combined with the symmetric and balanced
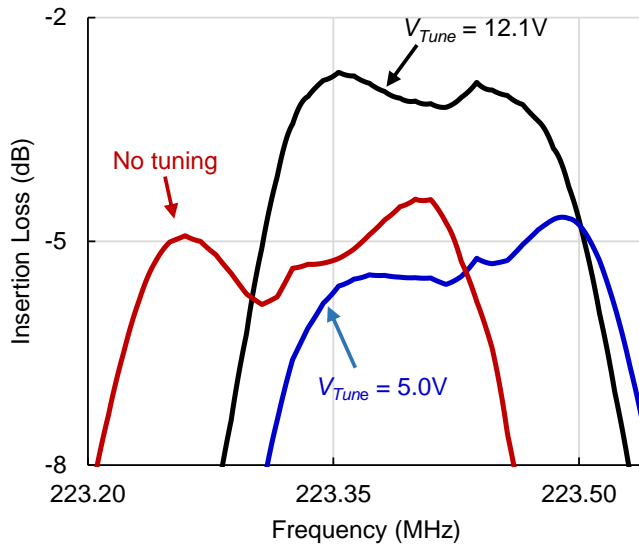
Fig. 10: Measured comparison of the terminated filter spectrum for varying tuning cases.

Fig. 11: Measured terminated spectrum over 50MHz span showing no strong spurious modes.

design lead to 50dB of out-of-channel rejection. Without symmetry and balance, a single-ended version of this filter suffers greatly from feedthrough that limits the stopband rejection to only 15dB. It also suffers from numerous mechanical spurious modes not seen in the differential measurement of Fig. 9.

Fig. 10 emphasizes the importance of electrical tuning for this tiny percent bandwidth filter by showing how proper tuning with 12.1V improves the passband shape and minimizes insertion loss. In particular, without tuning, the filter response exhibits as much as 2dB of passband ripple and 5dB of in-band insertion loss. After tuning, the passband ripple drops to the designed 0.5dB, and the insertion loss, as mentioned, improves by 2.3dB to 2.7dB. At the front-end of an RF circuit, improvement by 2.3dB makes a huge difference in receiver noise figure performance, so very much justifies the addition of dedicated frequency tuning devices.

Finally, Fig. 11 presents the terminated spectrum over a 50MHz wide span showing no strong spurious modes, again achieved by differential design and tuning.

VII. CONLCUSIONS

The combined 2.7dB passband insertion loss and 50dB stopband rejection of the demonstrated 206-element 0.09%-bandwidth 223.4-MHz differential micromechanical disk filter represents a landmark for capacitive-gap transduced micromechanical resonator technology. This demonstration proves that the mere introduction of small gaps, on the order of 39 nm, goes a long way towards moving this technology from a research curiosity to practical performance specs commensurate with the needs of actual RF channel-selecting receiver front-ends. It also emphasizes the need for tuning and defensive stress-relieving structural design when percent bandwidths and gaps shrink, all demonstrated by the work herein. Perhaps most encouraging is that the models used to design the filter and pre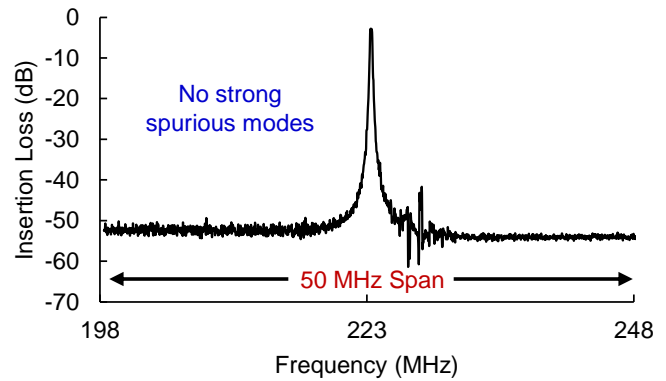dict its behavior seem to all be spot on. This means that predictions using these models foretelling 1-GHz filters with sub-200Ω impedances enabled by 20nm-gaps might soon come true, bringing this technology ever closer to someday realizing the ultra-low power channel-selecting communication front-ends targeted for autonomous set-and-forget sensor networks [6]. Work towards these goals continues.

VIII. REFERENCES

[1] S.-S. Li, Y.-W. Lin, Z. Ren, and C.-C. Nguyen, "An MSI micromechanical differential disk-array filter," in *Solid-State Sensors, Actuators and Microsystems Conference, 2007. TRANSDUCERS 2007. International*, 2007, pp. 307–311.

[2] C. Zuo, N. Sinha, M. B. Pisani, C. R. Perez, R. Mahameed, and G. Piazza, "Channel-Select RF MEMS Filters Based On Self- Coupled A1N Contour-Mode Piezoelectric Resonators," in *2007 IEEE Ultrasonics Symposium Proceedings*, New York, NY, USA, 2007, pp. 1156–1159.

[3] T.-T. Yen, C.-M. Lin, Y.-J. Lai, D. Wittwer, M. A. Hopcroft, and A. P. Pisano, "Fine frequency selection techniques for aluminum nitride Lamb wave resonators," in *Frequency Control Symposium (FCS), 2010 IEEE International*, 2010, pp. 9–13.

[4] R. Johnson, *Mechanical filters in electronics*. Wiley, 1983.

[5] J. R. Clark, W.-T. Hsu, M. A. Abdelmoneum, and C. T.-C. Nguyen, "High-Q UHF micromechanical radial-contour mode disk resonators," *J. Microelectromechanical Syst.*, vol. 14, no. 6, pp. 1298–1310, Dec. 2005.

[6] C.-C. Nguyen, "MEMS-based RF channel selection for true software-defined cognitive radio and low-power sensor communications," *Commun. Mag. IEEE*, vol. 51, no. 4, pp. 110–119, 2013.

[7] M. Akgul, L. Wu, Z. Ren, and C. Nguyen, "A Negative Capacitance Equivalent Circuit Model for Parallel-Plate Capacitive-Gap Transduced Micromechanical Resonators," *IEEE Trans. UFFC Accept. Publ. May 2014 Issue*.

[8] Y. Lin, W. C. Li, B. Kim, Y. W. Lin, Z. Ren, and C. T. . Nguyen, "Enhancement of micromechanical resonator manufacturing precision via mechanically-coupled arraying," in *Frequency Control Symposium, 2009 Joint with the 22nd European Frequency and Time forum. IEEE International*, 2009, pp. 58–63.

[9] H. C. Nathanson, W. E. Newell, R. A. Wickstrom, and J. R. Davis Jr, "The resonant gate transistor," *Electron Devices IEEE Trans. On*, vol. 14, no. 3, pp. 117–133, 1967.